Originally published as:

Baumann, G., Henninges, J. (2012): Sensitivity study of pulsed neutron-gamma saturation monitoring at the Altmark site in the context of CO2 storage. - Environmental Earth Sciences, 67, 2, 463-471

DOI: 10.1007/s12665-012-1708-x

Sensitivity study of pulsed neutron-gamma saturation monitoring at the Altmark site in the context of CO_2 storage

Gunther Baumann* and Jan Henninges

GFZ German Research Centre for Geosciences, Telegrafenberg, 14473 Potsdam, Germany

*corresponding author

Email baumann@gfz-potsdam.de

Phone +49 331 288 1970

Fax +49 331 288 1450

Abstract

The injection of CO_2 into depleted natural gas reservoirs has been proposed as a promising new technology for combining enhanced gas recovery and geological storage of CO_2. During the injection, application of suitable techniques for monitoring of the induced changes in the subsurface is required. Observing the movement and the changes in saturation of the fluids contained in the reservoir and the confining strata is among the primary aims here. It is shown that under conditions similar to the Altmark site, Germany, pulsed neuton-gamma logging can be applied with limitations. The pulsed neutron-gamma method can be applied for detection and quantification of changes in brine saturation and water content, whereas changes in the gas composition are below the detection limit. A method to account for the effects of salt precipitation resulting from evaporation of residual brine is presented.

Keywords: pulsed neutron-gamma logging, PNG, enhanced gas recovery, salt precipitation, water evaporation, Altmark gas field

1 Introduction

The injection of carbon dioxide (CO_2) into depleted natural gas reservoirs has been proposed as a promising new technology for combining enhanced gas recovery (EGR) and geological storage of CO_2 (van der Burgt et al. 1992). Application of this technology could both lead to environmental and economic benefits by reducing greenhouse gas emissions in the framework of carbon capture and storage (CCS) and increasing the amount of recoverable gas from a reservoir (Oldenburg et al. 2004). Since only few experiences from field-scale experiments do exist until now, the joint research project CLEAN (Kühn et al. 2011, 2012) for evaluation of the EGR potential at the Altmark site, Germany, which is owned and operated by GDF SUEZ E&P Deutschland GmbH (GDF SUEZ), has been set up.

During the proposed CO_2 injection process, application of suitable techniques for monitoring of the induced changes in the subsurface is required. For EGR, enabling a safe and reliable operation is of prime importance. In addition to this, the verification of the stored amount of CO_2 and observation of possible leakages from the intended storage formations are required in the context of CO_2 storage (Benson and Cook 2005). Existing models for the spreading of the CO_2, including the position and form of the injection front, as well as mixing of the different gases, need to be checked. The monitoring of the injection front enables to predict and control the breakthrough of CO_2 at production wells. Changes in water saturation can create new migration pathways, e.g. within previously flooded reservoir intervals, or indicate leakages through the confining strata of the caprock. Therefore, observing the movement and the changes in saturation of the fluids contained in the reservoir and the confining strata is among the primary aims for monitoring. Within this study, a geophysical well logging method for this purpose is evaluated for application under conditions similar to the Altmark site, which might be representative of many suitable locations for a commercial deployment of the EGR and CCS technologies worldwide.

For the assessment of static saturation conditions, a broad range of geophysical methods commonly applied during the exploration for oil and gas can be used. But for measurements in cased boreholes, which would be the standard situation encountered under the given conditions, only a limited number of techniques like pulsed neutron-gamma (PNG) logging are applicable.

Monitoring of saturation changes using PNG logging is widely used in oil and gas fields (e.g. Smolen 1996; Morris et. al. 2005). The PNG technique uses controlled neutron bursts, which interact with the nuclei of the surrounding borehole and formation. Due to the high contrast of the evaluated physical parameters between formation brine and gas, the PNG method has already been applied successfully for monitoring CO_2 injection in saline aquifers (e.g. Sakurai et. al. 2005; Müller et. al. 2007; Vu-Hoang et al. 2009). But since the contrast between gases is low, a decreased sensitivity to evaluate saturation changes in depleted gas fields can be expected. Furthermore the dissolution of brine into the flowing CO_2 stream, which is associated with the precipitation of salts, can affect the evaluation of PNG logs (Baumann et. al. 2011). Therefore, to assess the potential of the PNG method for conditions similar to the Altmark site, a sensitivity analysis considering salt precipitation was performed within this study.

2 Altmark saturation conditions, expected saturation changes and selection of PNG logging mode

The following describes the saturation conditions and possible changes in pore space fluid composition by dry CO_2 injection that then feed in a saturation model described by individual volumetric mixing equations.

The reservoir intervals above the initial gas-water contact (GWC) at the Altmark site are partially saturated with mobile natural gas (S_{ng}) and immobile water. The natural gas is predominantly composed of 0.75 N_2 and 0.25 CH_4 by volume (GDF SUEZ 2009). The irreducible water saturation (S_{wirr}) has been determined from logging data (GDF SUEZ 2009) and ranges between 0-40 % of the total porosity (ϕ_{tot}). Accordingly, the volume-weighted shares (fractions) of natural gas, irreducible water and the rock matrix result in the first case of the considered baseline model characterizing the section above the GWC.

Due to increased reservoir pressure during CO_2 injection, the initial GWC would be anticipated to move downward. Thus, formerly completely water-saturated injection layers are flooded with CO_2. Therefore, the baseline model below the initial GWC simplifies to a water-saturated pore space. In this second case, a similar distinction is made between irreducible immobile water and free mobile water.

Therefore in summary, two different cases for the baseline model before injection are considered: case 1 refers to the situation above the initial GWC (pore space partially saturated with natural gas and immobile water), and case 2 to the reservoir section below the initial GWC (completely water-saturated). Starting from the two different baseline saturation conditions and their individual phase mobilities, different physical mechanisms lead to saturation changes.

The mobile fluid fraction (case 1: natural gas, case 2: brine) is physically displaced by the injected CO_2. In contrast to that, the immobile fluid fraction (case 1 and case 2: brine) cannot be displaced. But dry injected CO_2 has some water evaporation capability, where the water is dissolved in the flowing CO_2 stream.

The evaporation of water causes an increase in the brine’s salt concentration until the temperature-dependent solubility limit is reached. Upon reaching the salt solubility, further water evaporation leads to salt precipitation.

Such salt precipitations associated with CO_2 flooding have already been proven in laboratory experiments (Wang et. al. 2009, 2010). Furthermore the precipitation of salt is known as a possible source of formation damage in gas producing wells (Kleinitz et. al. 2001).

Modeling results show that gravity-forced upflow of CO_2 and capillary-forced backflow of brine toward the injection point can also affect saturation changes and salt precipitation (Pruess and Müller 2009; Zeidouni et. al. 2009; Giorgis et. al. 2007). These processes can even increase the amount of precipitated salt over the originally dissolved salt load in areas close to the injection point in saline aquifers. Such effects, however, are not expected in a gas reservoir where the brine is already at irreducible saturation and hence immobile.

For CO_2 storage operations in nearly depleted gas fields like the Altmark site, the evaporation process associated with salt precipitations is relevant in the vicinity of an injection well, where dry CO_2 enters the reservoir. In contrast to that, in the vicinity of observation wells, it can be assumed that the arriving CO_2 is already water saturated. Therefore, only the mobile fluid fraction can be displaced here, but no water can be evaporated anymore.

In general, two different modes of PNG logging for saturation evaluation can be distinguished. In the Σ logging mode, the total macroscopic capture cross section SIGMA (Σ_{tot}) is determined from capture gamma ray spectra. After elastic and inelastic scattering, the neutrons are finally captured mainly by hydrogen and chlorine with a corresponding emission of gamma rays. Σ_{tot} is derived from the decline of gamma rays with time. In contrast to this, in C/O logging mode, the formation's carbon and oxygen concentrations, especially their ratio (COR), are determined from the inelastic gamma ray spectra (e.g. Smolen 1996).

Applicability of either the Σ or C/O methods is determined by analyzing the measurement contrast between the examined fluids. The C/O logging mode, for example is used to determine oil saturation in low salinity formations, since oil and freshwater have nearly the same Σ value. For the case considered here, low gas densities correspond to low carbon and oxygen concentrations as well as low Σ values. Moreover, natural gas (CH_4, N_2) and CO_2 contain carbon, but only CO_2 contains oxygen. Therefore, the fraction of natural gas displacement by CO_2 contributes only marginally to the total carbon or oxygen concentration and to the overall COR of the formation. Hence, both the changes in the total COR as well as the Σ value of the formation by displacement of natural gas by CO_2 can be considered to be low. But since the Σ contrast between CO_2 and brine is large, a good detectability of brine displacement can be expected in Σ logging mode, which is therefore more appropriate than C/O logging under the considered conditions. Regarding the evaporation processes associated with salt precipitation, the Σ contrast nevertheless only results from the difference between freshwater and CO_2, since the salt remains in the pore space. Details of the resulting differences are therefore evaluated in the following sensitivity study focusing on Σ logging.

3 Assumed saturation scenarios and saturation models

Σ_{tot} of a mixture of materials (minerals and fluids) results from the sum of the volume fraction (V_i) and the macroscopic capture cross section (Σ_i) of constituent i (Serra 1984)

$$\Sigma_{tot} = \sum_i V_i \cdot \Sigma_i$$

The simple volumetric mixing law considers the rock matrix and the fluid filled pore space. Depending on individual reservoir properties and expected saturation changes, individual expansions for multiple matrix (e.g. shale) or fluid (oil, gas, brine) components can be included in the mixing laws (Kimminau and Plasek 1992).

Since different processes lead to saturation changes, the total porosity is divided into fractions occupied by a mobile (effective porosity, ϕ_{eff}) and an immobile (irreducible porosity, ϕ_{irr}) phase. The pore space above the initial GWC ϕ_{eff} is saturated with natural gas (case 1) and below the GWC with brine (case 2). ϕ_{irr} results for both cases from $S_{wirr.}$

$$\phi_{tot} = \phi_{eff} + \phi_{irr}$$

with

$$\phi_{eff} = S_{ng/w} \cdot \phi_{tot}$$

and

$$\phi_{irr} = S_{w_{irr}} \cdot \phi_{tot}$$

where the subscripts ng and w correspond to the pore fluid components, natural gas and brine, respectively.

Accordingly, the volume-weighted shares of natural gas (case 1) or brine (case 2), the irreducible water and the rock matrix result in the baseline model (Figure 1, Baseline).

To estimate the effect of saturation changes on Σ measurements, the following two scenarios are assumed for repeat measurements during injection.

The first scenario takes only the physical in situ fluid displacement into account, where S_{wirr} is assumed to be unchanged (Figure 1, Scenario 1). The second scenario considers not only the in situ fluid displacement, but in addition the evaporation of the irreducible water (Figure 1, Scenario 2).

The saturation models are built up for the repeat scenarios during injection based on the volume-weighted share of the individual components of the matrix and the fluids contained in ϕ_{eff} and ϕ_{irr}. In a corresponding fashion, the total CO_2 saturation S_{CO2tot} results from the weighted sum of the individual CO_2 saturations S_{CO2eff} and S_{CO2irr} related to ϕ_{eff} or rather to ϕ_{irr} (Figure 1).

$$S_{CO_{2tot}} = S_{CO_{2eff}} \cdot \frac{\phi_{eff}}{\phi_{tot}} + S_{CO_{2irr}} \cdot \frac{\phi_{irr}}{\phi_{tot}}$$

The baseline model can be calculated as

$$\Sigma_{base} = (1 - \phi_{tot}) \cdot \Sigma_{ma} + \phi_{eff} \cdot \Sigma_{ng/w} + \phi_{irr} \cdot \Sigma_{w}$$

where the subscript ma corresponds to the rock matrix. Before injection, ϕ_{eff} is fully saturated with natural gas. Under the assumption that N_2 and CH_4 are completely miscible and can therefore be equally effectively displaced, Σ_{ng} results from the volume-weighted Σ values of N_2 and CH_4. (N_2 0.75 and CH_4 0.25 by volume, GDF SUEZ 2009).

To estimate the maximum expectable Σ changes for the sensitivity study, corresponding maximum possible saturation changes are evaluated in each scenario.

In the first scenario, the natural gas and brine in ϕ_{eff} is completely replaced by CO_2. Therefore, S_{CO2eff} is equal to one. Accordingly, the first scenario is calculated as follows

$$\Sigma_{rep-sc1} = (1 - \phi_{tot}) \cdot \Sigma_{ma} + \phi_{eff} \cdot \Sigma_{CO_2} + \phi_{irr} \cdot \Sigma_{w}$$

with S_{CO2tot}

$$S_{CO_{2tot}} = (1 - S_{ng}) \cdot \frac{\phi_{eff}}{\phi_{tot}}$$

In addition to the first scenario's parameters, the second scenario also takes into account the complete evaporation of irreducible water and resulting salt precipitation. Therefore, ϕ_{irr} is extended by a salt precipitation term ($S_{salt}\Sigma_{salt}$) in order to account for the remaining salt content. The second scenario results in

$$\Sigma_{rep-sc2} = (1 - \phi_{tot}) \cdot \Sigma_{ma} + \phi_{eff} \cdot \Sigma_{CO_2} + \phi_{irr} \cdot \left(S_{salt}\Sigma_{salt} + S_{CO_{2irr}}\Sigma_{CO_2} \right)$$

where S_{salt} is the salt saturation and Σ_{salt} is the macroscopic capture cross section of the precipitated salts. S_{CO2tot} is derived as follows

$$S_{CO_{2tot}} = (1 - S_{ng}) \cdot \frac{\phi_{eff}}{\phi_{tot}} + (1 - S_{salt}) \cdot \frac{\phi_{irr}}{\phi_{tot}}$$

In addition to in situ fluid displacement and water evaporation associated with salt precipitation, also mineral trapping of CO_2 can possibly result in Σ_{ma} changes.

Beyer et al. (2012) studied the reactive transport by CO_2 injection, including dissolution and precipitation kinetics of mineral reactions. Notable mineral trapping of CO_2 by carbonate precipitation starts after approximately 2000 years for the conditions similar to the Altmark site. Even over a period of 10000 years, the injected CO_2 results in dissolution of the primary silicates associated with the precipitation of clay minerals.

In contrast to the timescale of mineral trapping, displacement and evaporation processes occur more or less simultaneously with the CO_2 injection process. Resulting from these different timescales mineral dissolution and precipitation are not considered in the sensitivity study. Therefore, Σ_{ma} is assumed to be invariant for the sensitivity study.

3.1 Determination of pore fluid capture cross sections and salt precipitations

According to the saturation models, the involved pore fluid capture cross sections are analyzed in detail. Moreover, to assess the influence of salt precipitation on Σ measurements, the chemical brine composition from the Altmark site (De Lucia et al. 2012) is considered.

To calculate the Σ values of the pore fluids, the Σ calculation of molecules is introduced. The macroscopic capture cross section (Σ_i) in c.u. (1000 cm^{-1}) for a molecule i (mineral or fluid) is defined as the product of the mass-normalized microscopic capture cross section σ_{mi} in cm^2/g and the bulk density (ρ_b) in g/cm^3 (e. g. Ellis and Singer 2008)

$$\Sigma_i = \rho_b \cdot \sigma_{m_i}$$

The mass-normalized microscopic capture cross sections are calculated based on the microscopic capture cross sections from Sears (1992).

The capture cross section for brine (Σ_w) results from the sum of the fresh water capture cross section (Σ_{H2O}) and the dissolved salts (Σ_{salt})

$$\Sigma_w = \Sigma_{H2O} + \Sigma_{salt}$$

If the salt concentration c is given in grams per liter of solution (g/l) for all salts i, Σ_{salt} is calculated by

$$\Sigma_{salt} = \sum_i c_i \cdot \sigma_{m_i}$$

and Σ_{H2O}

$$\Sigma_{H2O} = \left(\rho_w \cdot 1000 - c_{salt}\right) \cdot \sigma_{m_{H2O}}$$

where ρ_w is the brine density (1.239 g/cm³, ambient conditions; GDF SUEZ 2009) and c_{salt} is the total dissolved salt concentration in g/l.

Similar to many brines from the North German Basin, the Altmark brine is dominated by chlorine. Since chlorine has a large σ_{mi} in comparison to other typical dissolved ions, the Σ chlorine fraction is dominant. The trace elements boron and lithium only play a subordinate role in the total solution content. But due to their considerably large σ_{mi}, their contribution to Σ_{salt} is not irrelevant. Overall, Σ_{salt} results in 136.26 c.u., where chlorine contributes 89.9 %, boron 6.9 % and lithium 2.0 % to the total value. All other remaining ions contribute less than 1.2 % to the total value.

Since chlorine is the dominant chemical constituent, the saturation state calculations are simplified. We represent Σ_{salt} only by a NaCl-equivalent concentration (c_{NaCl}). Therefore, the corresponding Σ_{NaCl} is equal to Σ_{salt}. This is a common assumption made in PNG interpretation (e.g. Smolen 1996; Serra 1984). In comparison to the "true" total salt concentration (347.18 g / l; Table 1), c_{NaCl} results in 388.59 g/l NaCl. c_{NaCl} is greater than the "true" total salt concentration. This results from the larger σ_{mi} of the trace elements boron and lithium compared to chlorine. Compensation for this discrepancy is made by increasing the NaCl-equivalent concentration until it reaches the total Σ_{salt} value.

The brine density for the NaCl-equivalent concentration under ambient conditions (25°C, 1 bar) was calculated by an analytical function dependent on pressure and temperature after Rowe and Chou (1970). The calculated NaCl-equivalent brine density of 1.239 g/cm³ under ambient conditions is similar to the "true" brine density. To account for the Altmark reservoir conditions (125 °C, 40 bar; GDF SUEZ 2009), the brine density was also adjusted after Rowe and Chou (1970) to 1.180 g/cm³. The decreasing brine density under reservoir conditions correspondingly results in a smaller NaCl-equivalent concentration of 369.92 g/l. Accordingly, Σ_w results in 147.73 c.u. In Table 1 all relevant brine parameters are summarized. The NaCl-equivalent brine under reservoir conditions is used for the halite precipitation calculation and the sensitivity study in the following section.

The gases' Σ values (Table 2) were also calculated for the reservoir conditions by adjusting the input densities as a function of pressure and temperature using the approach of Afeefy et. al. (2005).

The precipitation of all dissolved NaCl in a solution would yield a halite saturation (S_{NaCl}) of

$$S_{NaCl} = \frac{\rho_w \cdot X_{NaCl}}{\rho_{NaCl}} = \frac{c_{NaCl}}{1000 \cdot \rho_{NaCl}}$$

where X_{NaCl} is the mass fraction of dissolved NaCl in brine, c_{NaCl} is the NaCl concentration in g/l and ρ_{NaCl} is the NaCl density (extended after Battistelli 1997).

NaCl-equivalent concentration under reservoir conditions, S_{NaCl} , is 0.17 (ρ_{NaCl} = 2.17 g/cm³; Serra 1984), with a corresponding S_{CO2irr} of 0.83 (1- S_{NaCl}).

In the second scenario, where NaCl-equivalent concentrations have been introduced, the calculation of the salt term is limited to NaCl. This gives the following relation for Σ_{salt}

$$\Sigma_{salt} = c_{NaCl} \cdot \sigma_{m_{NaCl}} = S_{NaCl} \cdot \Sigma_{NaCl}$$

From the PNG methodic point of view, the relation demonstrates that the precipitated halite results in the same Σ reading as the corresponding dissolved NaCl in brine. Therefore, it does not matter for the Σ reading whether the salt is dissolved or precipitated. But in order to account for the porosity reduction caused by the salt precipitation, it is necessary to include S_{NaCl} in the saturation model.

4 Sensitivity study for the Altmark site

Monitoring of saturation changes is usually performed in time-lapse mode, comparing baseline measurements before injection with repeat measurements during injection. To evaluate the assumed saturation models, hypothetical Σ values based on the assumed cases and scenarios were calculated.

Case 1 describes the baseline above and case 2 the baseline below the initial GWC. Accordingly, the baseline measurement response was calculated (Table 2, S_{base}, case 1, case 2). The hypothetical repeat measurement response was calculated according to the first and second scenarios (Table 2, S_{sc1}, S_{sc2}). The first scenario takes only the physical in situ fluid displacement into account (Figure 1, scenario 1). The second scenario considers in addition the evaporation of the irreducible water (Figure 1, scenario 2). Subsequently, the differences between baseline and repeat measurements are analyzed.

To investigate the general behavior of the assumed cases and scenarios, first hypothetical baseline and repeat measurements were calculated as a function of the total porosity ϕ_{tot}. S_{wirr} was set to 50 % of ϕ_{tot}; therefore, ϕ_{eff} and ϕ_{irr} are equal. The Σ fluid values under reservoir conditions are used and the Σ matrix value (Σ_{ma}) corresponds to clean sandstone (10 c.u.; Smolen 1996). It should be noted that an inert matrix was assumed. Therefore, the choice of Σ_{ma} is generally irrelevant for the sensitivity study, since Σ_{ma} is constant for all baseline and repeat measurements.

4.1 Case 1: above the initial GWC

As expected, Σ increases for the baseline as well as for the two scenarios with increasing ϕ_{tot} (Figure 2, left ordinate). Also, the Σ differences between the baseline and the two scenarios (Diff(b-sc1), Diff(b-sc2)) increase with ϕ_{tot}. Diff(b-sc1) is much smaller than Diff(b-sc2) (Figure 2, right ordinate). For the maximum investigated total porosity of 0.5, Diff(b-sc1) results in 0.6 c.u. and Diff(b-sc2) in 5.1 c.u. The small Diff(b-sc1) result from the small Σ difference between natural gas and CO_2, since the irreducible water saturation remains unchanged in the first scenario. For the second scenario, the influence of evaporation associated with higher Σ differences between water and CO_2 is evident.

Based on the irreducible water saturation and the given scenarios, the total CO_2 saturation (S_{CO2tot}) results from the volume-weighted sum of the individual CO_2 saturations in ϕ_{eff} and ϕ_{irr}. Therefore, S_{CO2tot} for the first scenario (S_{sc1}) is 0.5 corresponding to S_{wirr} of 50 % of ϕ_{tot}. For the second scenario (S_{sc2}), S_{CO2tot} is 0.915 (Figure 4, right ordinate). This greater CO_2 saturation results from the additional volume fraction initially occupied by water, which is then evaporated and replaced by CO_2 in the second scenario. Correspondingly, the remaining volume fraction (1- S_{CO2tot}) is occupied by precipitated halite. Generally, ϕ_{tot} does not influence the saturation values, because the CO_2 volume increases proportional with ϕ_{tot}.

4.2 Case 2: below the initial GWC

Similar to case 1, Σ and the corresponding Σ differences in case 2 increase also for the baseline with increasing ϕ_{tot} (Figure 3). Also, the difference between the baseline and the first scenario is smaller than the difference between the baseline and the second scenario. For the maximum investigated total porosity of 0.5, Diff(b-sc1) results in 36.9 c.u., and Diff(b-sc2) is 41.4 c.u. These differences are an order of magnitude larger than for the natural gas saturated model (case 1). Case 1 and case 2 differ in the mobile fluid fraction that can be displaced by the injected CO_2. Below the initial GWC (case 2) the larger Σ difference between brine and CO_2 results in larger Σ differences between the baseline and two scenarios.

The influence of evaporation is of course similar for both cases below and above the GWC, since the same scenario is assumed. Therefore, the difference between (Diff(b-sc2)) and (Diff(b-sc1)) is the same and results in 4.5 c.u.

Also, the total CO_2 saturation (S_{CO2tot}) is equal for both cases but differs between the two scenarios. In the first scenario, only the mobile fluid fraction can be displaced and is occupied by the injected CO_2. The second scenario considers in addition the evaporation of the irreducible water resulting in an extra CO_2 saturated porosity fraction (ϕ_{irr}).

To illustrate the influence of neglecting potential salt precipitation on the estimated CO_2 saturation, we now focus on the immobile irreducible porosity fraction (ϕ_{irr}). Σ baseline simplifies to

$$\Sigma_{base\,irr} = \phi_{irr} \cdot \Sigma_w$$

and the Σ repeat value is calculated based on the second scenario focused on the evaporation process only.

$$\Sigma_{rep-sc2_{irr}} = \phi_{irr} \cdot \left(S_{salt}\Sigma_{salt} + S_{CO_{2irr}}\Sigma_{CO_2}\right)$$

where the subscript “irr” describes that the calculation considers ϕ_{irr} only. In combination with the equations for the calculation of the pore fluid capture cross sections, the inverted model solved for S_{CO2irr} results in

$$S_{CO_{2irr}} = \frac{1}{\Sigma_{CO_2}} \cdot \left(\Sigma_{H_2O} - \frac{\Sigma_{base_{irr}} - \Sigma_{rep-sc2\,irr}}{\phi_{irr}} \right)$$

S_{CO2irr} is 0.830 and independent of ϕ_{irr}. The remaining porosity fraction (0.17) is occupied by halite. Correspondingly, S_{CO2irr} and S_{CO2eff} weighted by their corresponding porosity fraction result in a total CO_2 saturation S_{CO2irr} of 0.915 as described above.

Conventional PNG saturation models assume displacement processes, which are included by individual expansions for multiple fluid components in the mixing laws (Kimmenau and Plasek 1992). Physically, it is not possible to displace the immobile fluid fraction. But assuming an inverted model where the irreducible water is not evaporated but displaced, S_{CO2irr} can be calculated from

$$S_{CO_{2irr}} = \frac{\Sigma_{base_{irr}} - \Sigma_{rep-sc2_{irr}}}{\phi_{irr} \cdot \left(\Sigma_w - \Sigma_{CO_2}\right)}$$

Here, an “apparent” S_{CO2irr} of 0.122 is calculated, opposed to a value of 0.830 using the inverted model of the second scenario. Neglecting the evaporation process and assuming a displacement process would therefore result in an erroneous underestimation of the CO_2 saturation. Therefore, it is important to account for the dry CO_2 evaporation capability by a saturation model which is extended by a salt precipitation component.

The following sensitivity study focuses on an injection well at the Altmark site since both natural gas displacement and evaporation of irreducible water can occur. An observation well is not taken into account separately, because the first scenario for an injection well is also representative for an observation well where only displacement processes can occur.

4.3 S13 injection well at the Altmark site

To assess whether saturation changes are to be expected at the Altmark site above the GWC are detectable with PNG monitoring; baseline (Table 2, S_{base}) and hypothetical repeat measurements according to the described scenarios (Table 2, S_{sc1}, S_{sc2}) were calculated for the S13 injection well. The log-derived total porosity and residual water saturation data of well S13 (GDF SUEZ 2009) were included. The assumed Σ values of the matrix correspond to clean sandstone (10 c.u.) in the injection layers and claystone (38 c.u.) in the non-injection intervals (Smolen 1996).

Due to the small Σ differences between the gases, the effect of gas displacement alone (scenario 1) is also correspondingly low (Figure 4). The largest contrast is 0.30 c.u. and occurs in the high porosity sandstone layers (X435-X455 m). The difference between the baseline and scenario 1 is in the range of typical PNG tool accuracy (0.21 c.u.; Plasek et. al. 1995) and would therefore not be detectable in practice.

Taking into account additional evaporation of irreducible water with the dissolved salts precipitating in the pore space (scenario 2), the calculated Σ contrast is an order of magnitude higher. As for the first scenario, the greatest contrast occurs in the high porosity sandstones with high irreducible water saturations, but for scenario 2, the difference is about 1.48 c.u. and could be detectable with typical PNG tools.

5 Conclusions

Application of the PNG method for estimation of saturation changes above the GWC is hampered under the considered conditions because of the low contrast between CO_2 and natural gas. The Σ contrast, taking into account only the gas displacement, is in the range of typical PNG tool accuracy and therefore not detectable. This is especially true for observation wells, since the arriving CO_2 is already water saturated. Only the mobile natural gas can be displaced, but the irreducible water saturation is unaffected.

Changes of the gas composition need to be quantified chemically, e.g. by analyzing samples of produced fluids in a laboratory or applying existing tools for downhole fluid analysis to quantify the CO_2 content in the reservoir fluids (Müller et. al. 2006).

Considering the evaporation processes associated with salt precipitation, which is expected to occur close to injection wells, the expected effect in the Σ reading is an order of magnitude larger than the effect of gas displacement alone. Potentially, evaporation effects could be monitored with PNG logs depending on the volume of irreducible water.

In general, it is important to take the water evaporation capability of dry CO_2 for injection wells into account. Conventional PNG saturation models based on displacement processes only would result in an erroneous underestimation of the CO_2 saturation.

Furthermore, changes in the GWC associated with a high Σ contrast between displaced brine and injected CO_2 can be detected very well.

Acknowledgements

This study was performed in the framework of the CLEAN project of the geoscientific research and development programme “GEOTECHNOLOGIEN” (publication number GEOTECH-1953 funded by the German Federal Ministry for Education and Research (BMBF).

References

Afeefy HY, Liebman JF, Stein SE (2005) Neutral Thermochemical Data, in NIST Chemistry WebBook. NIST Standard Reference Database Number 69, (Eds. P. J. Linstrom and W. G. Mallard), National Institute of Standards and Technology, Gaithersburg MD, 20899, (http://webbook.nist.gov)

Battistelli A, Calore C, Pruess K (1997) The simulator TOUGH2/EWASG for modeling geothermal reservoirs with brines and noncondensible gas. Geothermics 26(4):437-464, doi:10.1016/S0375-6505(97)00007-2

Baumann G, Henninges J, De Lucia M (2011) Sensitivity study of pulsed neutron gamma monitoring to evaluate saturation changes for depleted gas field conditions in the context of CO_2 storage. EGU Geophysical Research Abstracts, EGU General Assembly 2011 (Vienna, Austria) 13(EGU2011-3301-1)

Benson SM, Cook P (2005) Underground geological storage. In: Metz B, Davidson O, de Coninck HC, Loos M, Meyer LA (eds) IPCC Special Report on Carbon Dioxide Capture and Storage. Prepared by Working Group III of the Intergovernmental Panel on Climate Change. Cambridge University Press, Cambridge, UK, and New York, NY, USA, pp 195-276

Beyer C, Li D, De Lucia M, Kühn M, Bauer S (2012) Modelling CO2-induced fluid-rock interactions in the Altensalzwedel gas reservoir: Part II- coupled reactive transport simulation. Environmental Earth Sciences, doi:10.1007/s12665-012-1684-1

De Lucia M, Albrecht D, Bauer S, Beyer C, Kühn M, Nowak T, Pudlo D, Stadler S (2012) Modelling CO2-induced fluid-rock interactions in the Altensalzwedel gas reservoir: Part I- from experimental data to a reference geochemical model. Environmental Earth Sciences

Ellis D, Singer J (2008) Well Logging for Earth Scientists, 2nd edn. Springer, Dordrecht, Netherlands

GDF SUEZ (2009) Clean DMS Data Management System, GFZ German Research Centre for Geosciences

Giorgis T, Carpita M, Battistelli A (2007) 2D modeling of salt precipitation during the injection of dry CO2 in a depleted gas reservoir. Energy Conversion and Management 48(6):1816-1826, doi:10.1016/j.enconman.2007.01.012

Kimminau S, Plasek R (1992) The Design of Pulsed Neutron Reservoir Monitoring Programs. SPE Formation Evaluation 7(1):93-98, 20589-PA

Kleinitz W, Koehler M, Dietzsch G (2001) The Precipitation of Salt in Gas Producing Wells. SPE European Formation Damage Conference, p 7, 68953-MS

Kühn K, Tesmer M, Pilz P, Meyer R, Reinicke K, Förster A, Schäfer D, CLEAN Partners (2012) Overview of the Joint Research Project CLEAN: CO2 Large-Scale Enhanced Gas Recovery in the Altmark Natural Gas Field (Germany). Environmental Earth Sciences

Kühn M, Förster A, Großmann J, Meyer R, Reinicke A, Schäfer D, Wendel H (2011) CLEAN: Preparing for a CO2-based Enhanced Gas Recovery in a depleted gas field in Germany. Energy Procedia 4:5520-5526. doi:10.1016/j.egypro.2011.02.538

Morris C, Aswad T, Morris F, Quinlan T (2005) Reservoir Monitoring with Pulsed Neutron Capture Logs. SPE Europec/EAGE Annual Conference p 16, 94199-MS

Müller N, Elshahawi H, Dong C, Mullins OC, Flannery M, Ardila M, Weinheber P, Chinn McDade E (2006) Quantification of Carbon Dioxide Using Downhole Wireline Formation Tester Measurements. SPE Annual Technical Conference and Exhibition p 10, 100739-MS

Müller N, Ramakrishnan T, Boyd A, Sakruai S (2007) Time-lapse carbon dioxide monitoring with pulsed neutron logging. International Journal of Greenhouse Gas Control 1(4):456-472, doi:10.1016/S1750-5836(07)00071-0

Oldenburg CM, Stevens SH, Benson SM (2004) Economic feasibility of carbon sequestration with enhanced gas recovery (CSEGR). Energy 29 (9-10):1413-1422

Plasek R, Adolph R, Stoller C, Willis D, Bordon E, Portal M (1995) Improved Pulsed Neutron Capture Logging With Slim Carbon-Oxygen Tools: Methodology. SPE Annual Technical Conference and Exhibition p 15, 30598-MS

Pruess K, Müller N (2009) Formation dry-out from CO2 injection into saline aquifers: 1. Effects of solids precipitation and their mitigation. Water Resources Research 45(W03402):11, doi:10.1029/2008WR007101

Rowe AM, Chou JCS (1970) Pressure-volume-temperature-concentration relation of aqueous sodium chloride solutions. Journal of Chemical and Engineering Data 15:61-66

Sakurai S, Hovorka S, Ramakrishnan TS, Boyd A, Mueller N (2005) Monitoring Saturation Changes for CO2 sequestration: Petrophysical Support of the Frio Brine Pilot Experiment. SPWLA 46th Annual Logging Symposium p 16, 2005-YY

Sears VF (1992) Neutron scattering lengths and cross sections. Neutron News 3(3):29-37

Serra O (1984) fundamentals of well-log interpretation, vol 1. Elsevier Science Publishers B. V.

Smolen J (1996) Cased Hole and Production Log Evaluation. Pennwell Publishing Company, Tulsa, Oklahoma

van der Burgt MJ, Cantle J, Boutkan VK (1992) Carbon dioxide disposal from coal-based IGCC's in depleted gas fields. Energy Conversion and Management 33 (5-8):603-610. doi:10.1016/0196-8904(92)90062-2

Vu-Hoang D, Henninges J, Hurter S (2009) Monitoring carbon dioxide saturation through wireline logging techniques. EGU Geophysical Research Abstracts, EGU General Assembly 2009 (Vienna, Austria) 11(EGU2009-10051)

Wang Y, Mackie E, Rohan J, Luce T, Knabe R, Appel M (2009) Experimental study on halite precipitation during CO_2 sequestration. International Symposium of the Society of Core Analysis p 12, SCA2009-25

Wang Y, Luce T, Ishizawa C, Shuck M, Smith K, Ott H, Appel M (2010) Halite precipitation and permeability assessment during supercritical CO_2 core flood. International Symposium of the Society of Core Analysis p 12, SCA2010-18

Zeidouni M, Pooladi-Darvish M, Keith D (2009) Sensitivity Analysis of Salt Precipitation and CO2-Brine Displacement in Saline Aquifers. SPE International Conference on CO2 Capture, Storage, and Utilization p 16, 126690-MS

Figure captions

Fig. 1 Saturation models. Baseline: in situ saturation condition before injection. Scenario 1: physical natural gas / brine displacement in ϕ_{eff}. Scenario 2: physical natural gas displacement in ϕ_{eff} and complete evaporation of irreducible water volume ϕ_{irr} associated with salt precipitation.

Fig. 2 Σ modeling results (left ordinate) for the baseline above the initial GWC (case 1, Σ_b) and the two different scenarios (Σ_{sc1}, Σ_{sc2}) as a function of the total porosity (ϕ_{tot}) and the corresponding differences (right ordinate) between the baseline and two scenarios (Diff(b-sc1)), Diff(b-sc2)). The irreducible water saturation was set to 50 % of ϕ_{tot}.

Fig. 3 Σ modeling results (left ordinate) for the baseline below the initial GWC (case 2, Σ_b) and the two different scenarios (Σ_{sc1}, Σ_{sc2}) as a function of the total porosity (ϕ_{tot}) and the corresponding differences (right ordinate)

between the baseline and two scenarios (Diff(b-sc1)), Diff(b-sc2)). The irreducible water saturation was set to 50 % of ϕ_{tot}.

Fig. 4 Σ modeling results for the baseline and the two different scenarios for the S13 injection well at the Altmark site. Injection intervals with high permeabilities are indicated by dotted signature. Left panel: total porosity (phi_tot)* and effective porosity (phi_eff)*, middle panel: baseline (SIGM_b) and repeat Σ (SIGM_sc1, SIGM_sc2), right panel: difference between baseline and repeats (Diff_(b-sc1), Diff_(b-sc2)). * Data according to GDF SUEZ (2009).

Tables

Table 1 Capture cross sections for brine (Σ_w) as the sum of the capture cross sections of fresh water (Σ_{H2O}) and the dissolved salts (Σ_{salt}) for the “true” and the NaCl-equivalent brine under ambient (25°C, 1 bar) and reservoir conditions (125 °C and 40 bar) and the corresponding densities (ρ_w). The values have been rounded. * (data provided by GDF SUEZ 2009; adjusted by De Lucia et. al. this issue)

Brine	T [°C]; p [bar]	TDS [g/l]	ρ_w [g/cm³]	$\Sigma_{salt/NaCl}$ [c.u.]	Σ_{H2O} [c.u.]	Σ_w [c.u.]
“True” brine	25; 1	347.18*	1.239*	136.26	19.75	156.01
NaCl-eq. brine	25; 1	388.59	1.239	136.26	18.92	155.18
NaCl-eq. brine	125; 40	369.92	1.180	129.72	18.01	147.73

Table 2 Σ values of different fluids and the associated saturations for the baseline (S_{base}) and the two assumed scenarios (S_{sc1}, S_{sc2}). * Data according to GDF SUEZ (2009).

Fluid (125 °C, 40 bar)	**Σ [c.u.]**	**S_{base}, case 1 [V/V]**	**S_{base}, case 2 [V/V]**	**S_{sc1} [V/V]**	**S_{sc2}, [V/V]**	**ϕ [V/V]**
N_2	2.722	0.75*	0	0	0	ϕ_{eff}
CH_4	0.984	0.25*	0	0	0	
Natural Gas	**2.288**	**1**	**0**	**0**	**0**	
NaCl-eq. brine	**147.73**	**0**	**1**	**0**	**0**	
CO_2	0.003	0	0	1	1	
NaCl-eq. brine	147.73	1	1	1	0	ϕ_{irr}
NaCl	760.92	0	0	0	0.17	
CO_2	0.003	0	0	0	0.83	

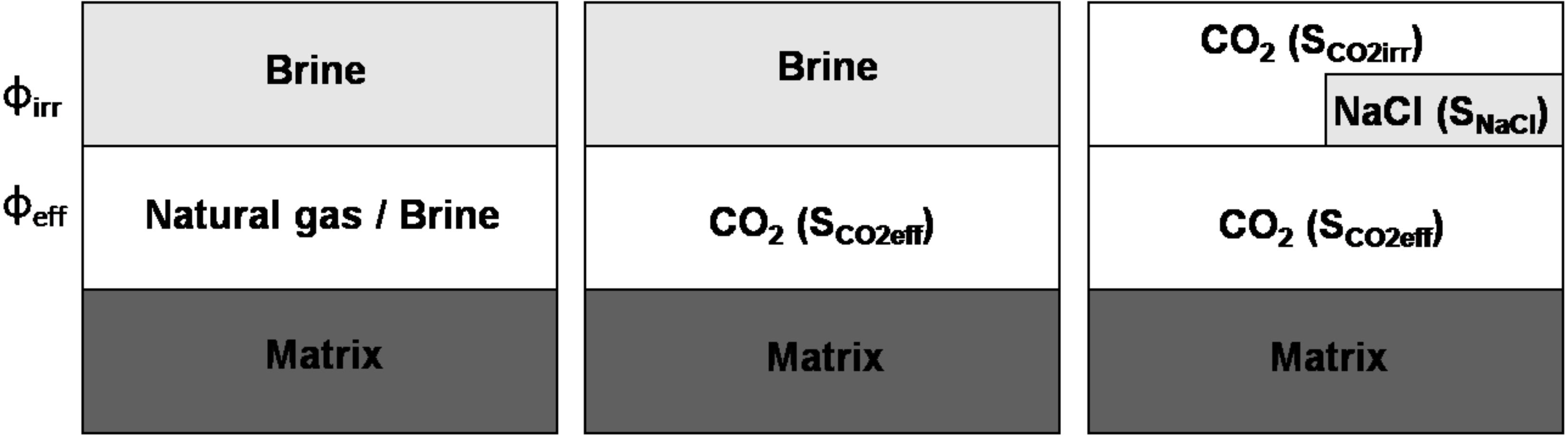
ϕ_{irr}
ϕ_{eff}
Brine
Natural gas / Brine
Matrix
Brine
CO_2 (S_{CO2eff})
Matrix
CO_2 (S_{CO2irr})
NaCl (S_{NaCl})
CO_2 (S_{CO2eff})
Matrix

Baseline

Scenario1

Scenario2

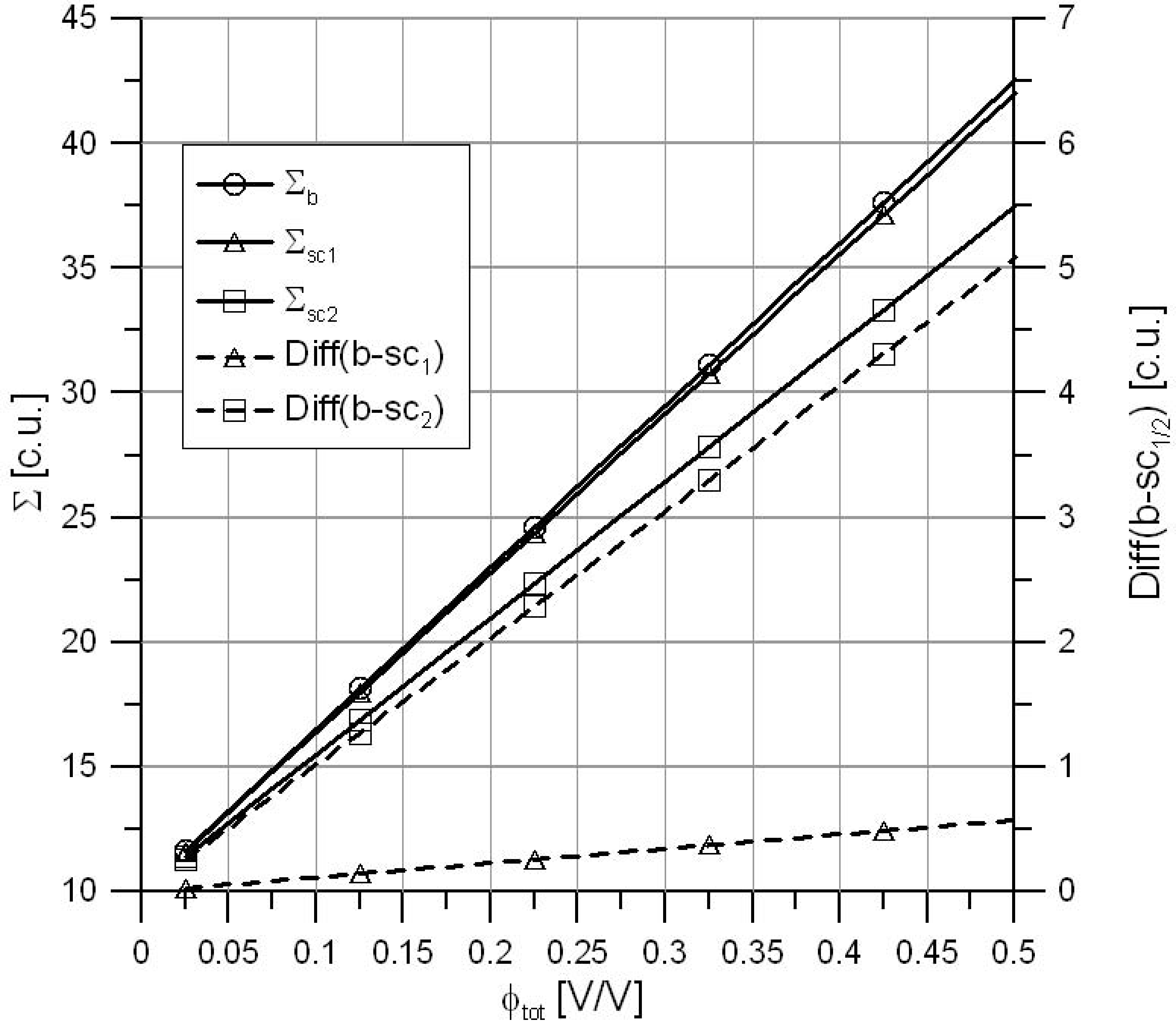

45
40
35
30
25
20
15
10
Σ [c.u.]
7
6
5
4
3
2
1
0
Diff(b-sc1/2) [c.u.]
0
0.05
0.1
0.15
0.2
0.25
0.3
0.35
0.4
0.45
0.5
ϕtot [V/V]
Σb
Σsc1
Σsc2
Diff(b-sc1)
Diff(b-sc2)

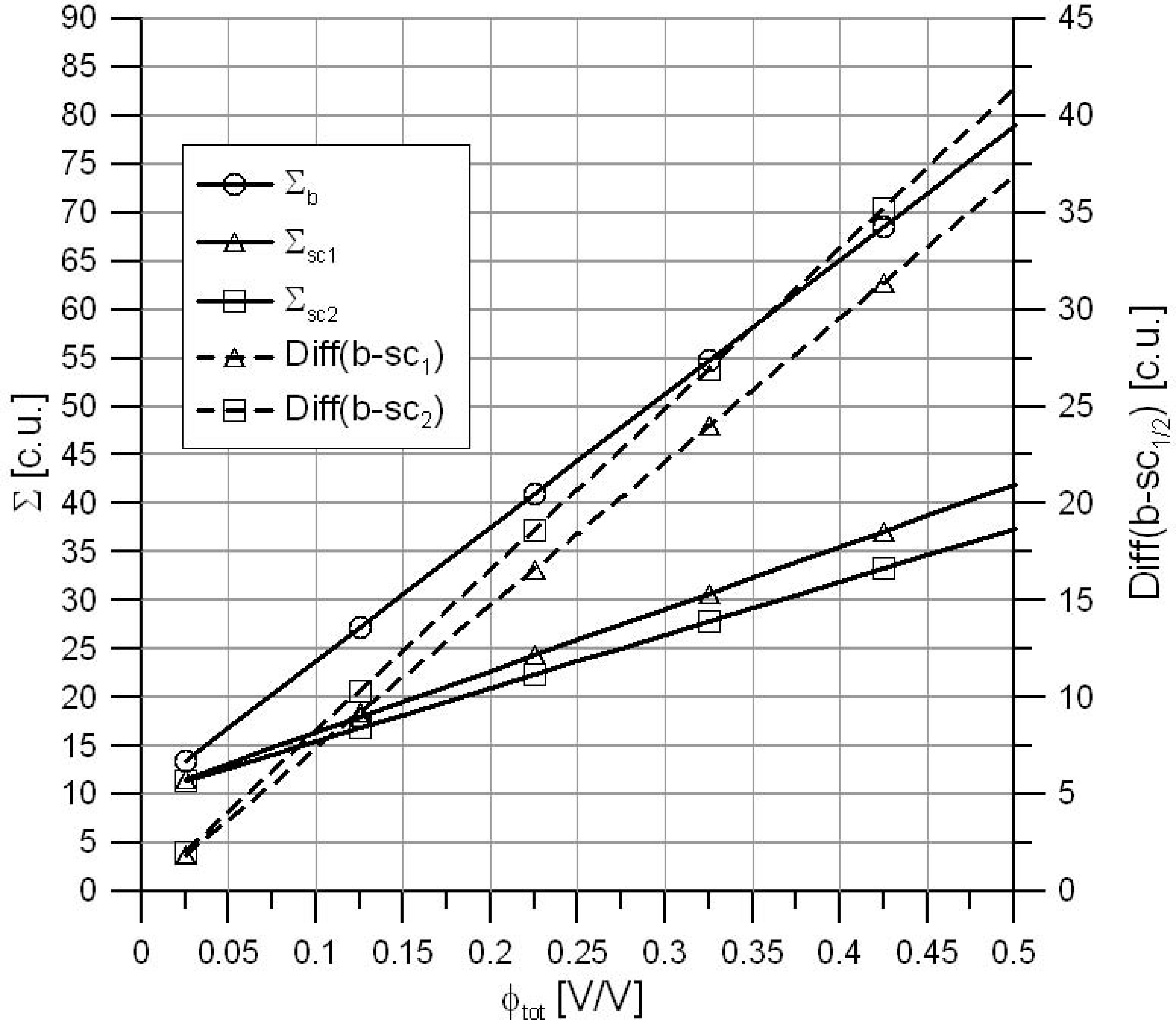
Σ [c.u.]
Diff(b-sc$_{1/2}$) [c.u.]
ϕ_{tot} [V/V]
Σ_b
Σ_{sc1}
Σ_{sc2}
Diff(b-sc$_1$)
Diff(b-sc$_2$)
0
5
10
15
20
25
30
35
40
45
50
55
60
65
70
75
80
85
90
0
5
10
15
20
25
30
35
40
45
0
0.05
0.1
0.15
0.2
0.25
0.3
0.35
0.4
0.45
0.5

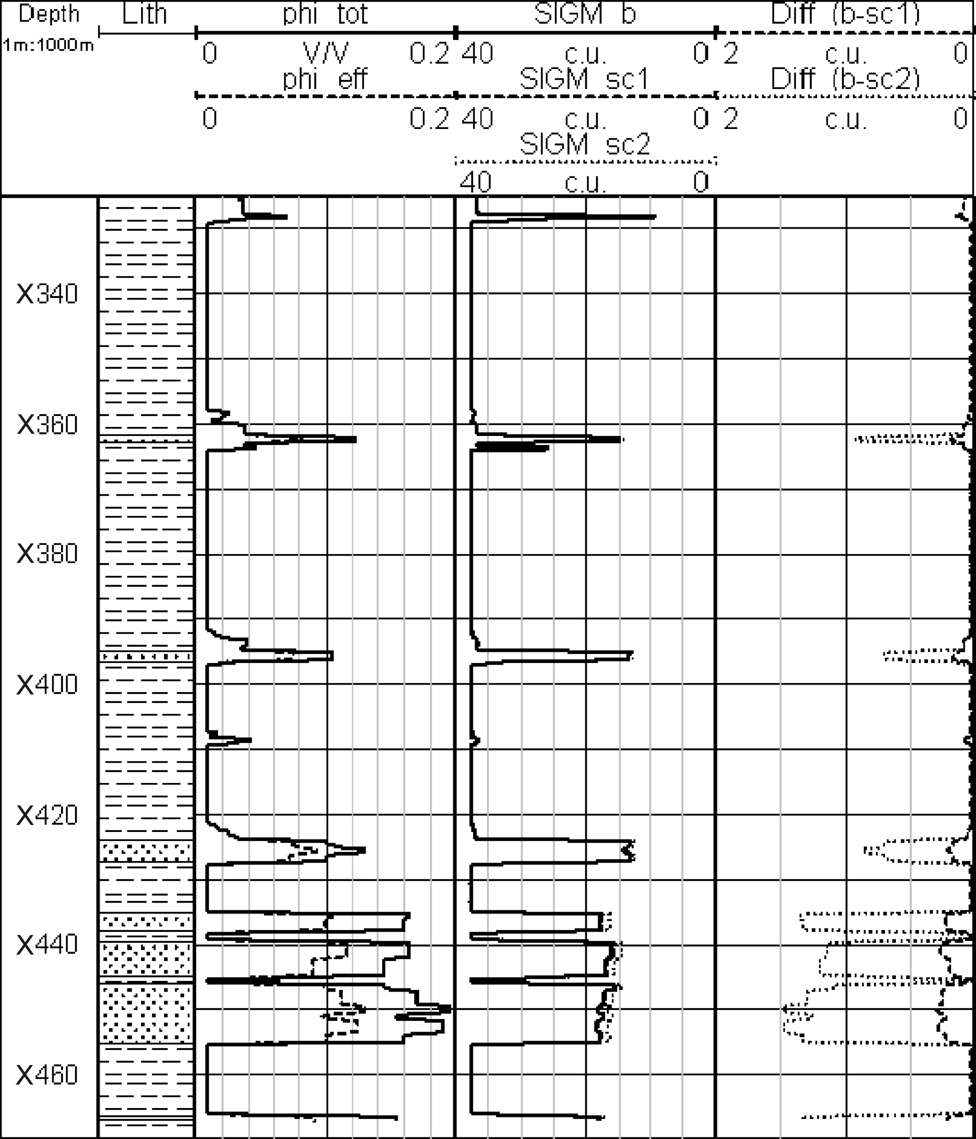
Depth
1m:1000m
Lith
phi tot
0 V/V 0.2
phi eff
0 0.2
SIGM b
40 c.u. 0
SIGM sc1
40 c.u. 0
SIGM sc2
40 c.u. 0
Diff (b-sc1)
2 c.u. 0
Diff (b-sc2)
2 c.u. 0
X340
X360
X380
X400
X420
X440
X460